Nanorods Hot Paper

Deutsche Ausgabe: DOI: 10.1002/ange.201505442
Internationale Ausgabe: DOI: 10.1002/anie.201505442

# A Unique Ternary Semiconductor–(Semiconductor/Metal) Nano-Architecture for Efficient Photocatalytic Hydrogen Evolution

*Tao-Tao Zhuang, Yan Liu, Meng Sun, Shen-Long Jiang, Ming-Wen Zhang, Xin-Chen Wang, Qun Zhang, Jun Jiang,* and Shu-Hong Yu**

***Abstract:*** *It has been a long-standing demand to design hetero-nanostructures for charge-flow steering in semiconductor systems. Multi-component nanocrystals exhibit multifunctional properties or synergistic performance, and are thus attractive materials for energy conversion, medical therapy, and photoelectric catalysis applications. Herein we report the design and synthesis of binary and ternary multi-node sheath hetero-nanorods in a sequential chemical transformation procedure. As verified by first-principles simulations, the conversion from type-I ZnS-CdS heterojunction into type-II ZnS-(CdS/metal) ensures well-steered collections of photo-generated electrons at the exposed ZnS nanorod stem and metal nanoparticles while holes at the CdS node sheaths, leading to substantially improved photocatalytic hydrogen-evolution performance.*

At nanoscale, material shape and composition directly influence function.[1] Fabricating multiple components in a single nanosystem has recently attracted great interest as result of the multifunctional properties or synergistic performance induced by heterointerfaces of the nanostructure.[2] Multi-component nanocrystals (hetero-nanostructures) with heterojunctions, allowing electron and hole transport and confinement to be controlled independently, form the basis of several optoelectronic applications.[3] Type-II heterojunctions, enabling accumulation of opposite charges at two sides, allow efficient electron–hole separation for optoelectronic applications. The development of hybrid nanostructures increases the level of structural-architectural sophistication.[4] The colloidal technique, benefitting from adjusting the energy of solution/solid interface induced by various ligands, promotes the synthesis of elaborate hetero-nanostructures in the solution.[5]

Cation exchange strategy has proven to be particularly powerful for accessing the nanocrystals which are difficult to obtain by direct hot-injection synthetic methods.[6] In particular, the partial cation-exchange reaction, which circumvents separate nucleation and transfers a portion of the nanocrystal into a new composition, is a versatile method to prepare heterostructured ionic nanocrystals.[7] To date, several heterostructured nanocrystals based on wurtize (WZ) cadmium chalcogenide have been prepared by partial cation exchange.[8] Nevertheless, to develop a general and summative partial-exchange strategy for the synthesis of novel and well-defined multi-component metal sulfide nanocrystals remains elusive. Furthermore, the construction of more sophisticated colloidal hetero-nanostructures with targeted performance requires a high degree of synthetic ingenuity and creativity.

Herein, we constructed unique one-dimensional (1D) binary -[S1-S2]-S1-[S1-S2]-S1- and ternary -[S1-(S2/M)]-S1-[S1-(S2/M)]-S1- hetero-nanorods with segmented node sheaths S2 decorated by M (S1 = ZnS; S2 = CdS; M = Au, Pd, Pt) through the colloidal technique. The ternary hybrids were prepared by the post-synthetic modification of binary multi-node sheath -[ZnS-CdS]-ZnS-[ZnS-CdS]-ZnS- hetero-nanorods, which were transformed from single component ZnS nanorods by sequential cation exchange. In contrast to the cation-exchange process based on WZ cadmium chalcogenide described previously, we show that zinc blende (ZB) ZnS can also be the starting material for the synthesis of unique hetero-nanostructures by cation exchange, which enriches the synthesis of multi-component nanocrystals with diverse phase structures. Compared to the traditional core–shell or simple multiple hybrids, the structural characteristic of 1D multi-node sheath gives rise to increased availability for light absorption and continuity for charge transportation. More importantly, the selective growth of metal on a semiconductor with a smaller band gap (CdS node sheath) provided by the binary hetero-nanostructures results in the formation of a type-II heterojunction through the Fermi-level alignment. This structure ensures the delivery of photo-generated electrons from the CdS node sheath not only to the metal surface but also to the exposed ZnS stem, promoting the separation of electron and hole carriers. The charge-separation efficacy in this unique ternary nanosystem leads to

[*] T. T. Zhuang,[+] M. Sun, Prof. Dr. S. H. Yu
Division of Nanomaterials & Chemistry, Hefei National Laboratory for Physical Sciences at Microscale, Collaborative Innovation Center of Suzhou Nano Science and Technology, Department of Chemistry
University of Science and Technology of China
Hefei, Anhui 230026 (P.R. China)
E-mail: shyu@ustc.edu.cn
Homepage: http://staff.ustc.edu.cn/~yulab/

Y. Liu,[+] S. L. Jiang, Prof. Dr. Q. Zhang, Prof. Dr. J. Jiang
Department of Chemical Physics, Synergetic Innovation Center of Quantum Information and Quantum Physics, Collaborative Innovation Center of Chemistry for Energy Materials (iChEM)
University of Science and Technology of China
Hefei, Anhui 230026 (P.R. China)
E-mail: jiangj1@ustc.edu.cn

M. W. Zhang, Prof. Dr. X. C. Wang
Research Institute of Photocatalysis, Fujian Provincial Key Laboratory of Photocatalysis, State Key Laboratory Breeding Base, College of Chemistry and Chemical Engineering, Fuzhou University
Fuzhou, Fujian 350002 (P.R. China)

[+] These authors contributed equally to this work.

Supporting information for this article is available on the WWW under http://dx.doi.org/10.1002/anie.201505442.

 © 2015 Wiley-VCH Verlag GmbH & Co. KGaA, Weinheim 

the performance improvement of photocatalytic hydrogen evolution.

We started with the ZnS-CdS hybrids, as both are well established and widely investigated nanosystems. The hetero-nanostructures composed of ZnS and CdS exhibit good absorption of ultraviolet and visible light (Figure S1 in the Supporting Information). The band gaps of ZnS (ca. 3.6 eV) and CdS (ca. 2.4 eV) span both the oxidation and reduction potentials of water splitting reaction (Figure S2a), as confirmed by computed density of states (DOS) of atomic models (Figure S2b,c). The calculated workfunctions of ZnS(111) and CdS(111) facets are close, suggesting good contacts and electronic couplings at interface (Figure S2d). Scheme 1-I shows a summary of major cation-exchange processes involved in the formation of binary multi-node sheath hetero-nanorods. Colloidal binary ZnS–CdS hetero-nanorods with segmented CdS node sheaths were prepared using chemical transformation, involving two steps: i) synthesis of -[ZnS-$Ag_2S$]-ZnS-[ZnS-$Ag_2S$]-ZnS- hetero-nanorods through partial Zn/Ag exchange from ultrathin ZnS nanorods and ii) transformation to -[ZnS-CdS]-ZnS-[ZnS-CdS]-ZnS- by complete Ag/Cd exchange. The formation of multi-node sheath ZnS–$Ag_2S$ hetero-nanorods is thermodynamically driven by the different solubility product constant between $Ag_2S$ and ZnS in methanol solvent. The $Zn^{2+}$ ion is a harder acid than $Ag^+$ owing to its smaller radius and higher charge density than $Ag^+$. According to the hard–soft acid–base theory, ZnS is preferentially solvated relative to $Ag_2S$ in the polar solvent (hard base).[9] Such partial cation-exchange manipulation of the solution equilibrium at room temperature would allow self-limiting substitution, resulting in a rod–sheath structure different to the previously reported CdS-$Ag_2S$ segmented superlattice.[8a] The transformation from multi-node sheath ZnS-$Ag_2S$ to multi-node sheath ZnS-CdS is favored by the addition of $Cd^{2+}$ ions, along with tributylphosphine (TBP). TBP, as a soft base, preferentially strongly binds to the monovalent $Ag^+$ ions to form a dative bond as well as a bonds to S to reduce the bonding energy between Ag and S, which can lead to the replacement of soft $Ag^+$ in the $Ag_2S$ node sheath with hard divalent $Cd^{2+}$ metal ions.[6a] Ternary -[ZnS-(CdS/Au)]-ZnS-[ZnS-(CdS/Au)]-ZnS- hetero-nanostructures were prepared through the post-synthetic modification of pre-made binary ZnS-CdS hetero-nanorods (Scheme 1-II). In a typical synthesis of Au nanocrystals, a quantity of ZnS-CdS was added as seeds at the initial stage of reaction to obtain the selective surface growth with Au nanoparticles being grown only on CdS node sheaths (Scheme 1-II).

To determine the structure of binary ZnS-CdS hybrids, we performed first a detailed study on how the synthetic parameters modulate the growth of ZnS-$Ag_2S$ hetero-nanostructures (Figure S3). TEM, HRTEM, and HAADF-STEM images (Figure S3a–e) reveal the shape of multi-node sheath product. X-ray diffraction (XRD) patterns (Figure S3f) confirm the presence of cubic ZnS and monoclinic $Ag_2S$. Energy dispersive spectroscopy (EDS) spectra (Figure S3g) show that some of the $Zn^{2+}$ was exchanged by $Ag^+$. The evolution of ZnS-$Ag_2S$ hetero-nanorods was examined by treating the initial ZnS nanorods with $AgNO_3$/methanol solutions of various concentrations (Figure S4), understood in terms of Ostwald ripening. The node-sheath number depends on the actual length of the original ZnS nanorods. The TEM images of ZnS-$Ag_2S$ hetero-nanorods with different $Ag_2S$ node-sheath numbers, obtained through partial cation exchange when starting from the ZnS nanorods of different lengths, is demonstrated in Figure S5. Figure S6 shows the statistic result.

When growing from ZnS-$Ag_2S$ hetero-nanorods, binary ZnS-CdS can be constructed. Figure 1 presents the structural characterizations of the ZnS-CdS hetero-nanorods. The TEM image in Figure 1b shows the product is a segmented node nanorod (large-field view in Figure S7), in analogy to the initial ZnS-$Ag_2S$. Figure 1c displays bright nodes and dark stems for the structure of hetero-nanorods using HAADF-STEM. The high-resolution STEM image (Figure 1d) of the node corresponding to the hetero-nanorod in Figure 1c reveals the (111) plane of CdS. The STEM image in Figure S8 also shows the planes of binary hetero-nanorods. To clarify

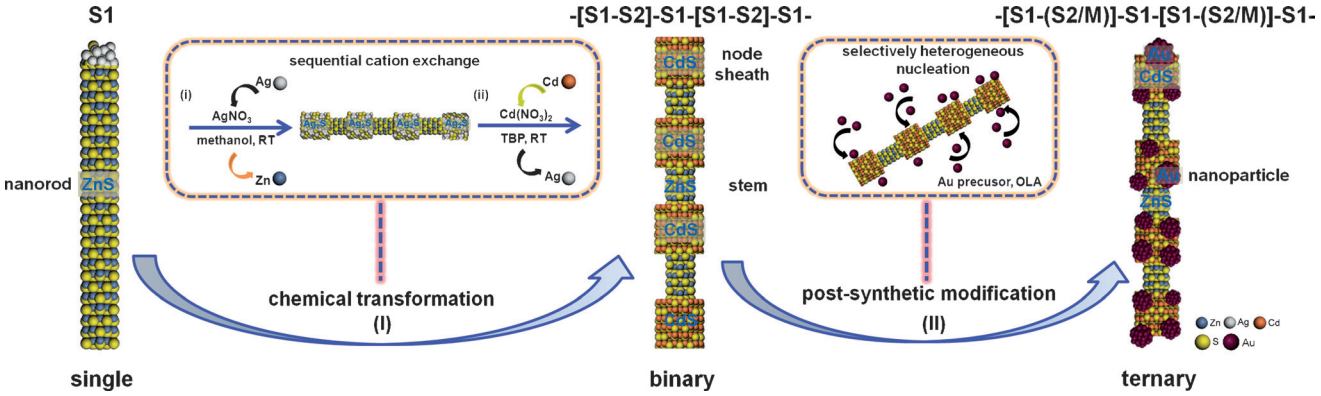


***Scheme 1.*** Schematic illustration of the evolution process from I) single component S1 to binary components S1-S2 by sequential cation exchange at room temperature: i) multi-node sheath ZnS-$Ag_2S$ hetero-nanorods formation through partial cation exchange from $Zn^{2+}$ to $Ag^+$ in ZnS nanorods; ii) multi-node sheath ZnS-CdS hetero-nanorods formation by complete exchange from $Ag^+$ to $Cd^{2+}$ along with tributylphosphine (TBP). II) Transformation into ternary components S1-(S2/M) with M being grown only on the S2 domains by post-synthetic modification of ZnS-CdS in oleylamine (OLA) reaction solution (S1 = ZnS, S2 = CdS, M = Au).


© 2015 Wiley-VCH Verlag GmbH & Co. KGaA, Weinheim

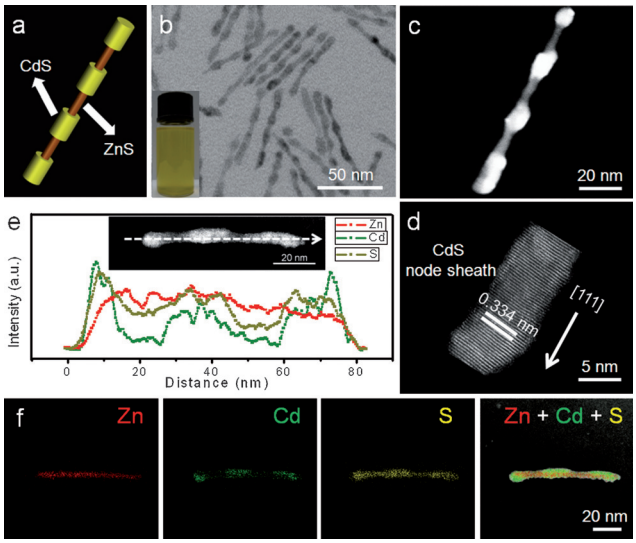


***Figure 1.*** a) Representative geometric model of binary hetero-nanorods with four CdS node sheaths. b) TEM image of ZnS-CdS. Inset: photograph of colloidal hetero-nanorods dispersed in toluene. c),d) HAADF-STEM images of hetero-nanorods. e) Smoothing simulation EDS line scan analysis and f) EDS mapping images, show the unique segmented node-sheath structure.

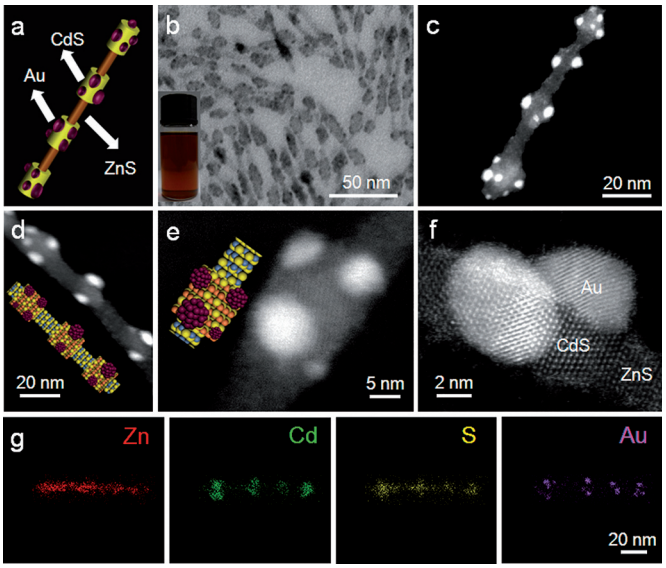


***Figure 2.*** a) Representative geometric model of ternary hetero-nanorods with four CdS node sheaths. b) TEM image of ZnS-(CdS/Au). Inset: photograph of colloidal hetero-nanorods dispersed in toluene. c–f) HAADF-STEM images of hetero-nanorods. g) EDS mapping images revealing the site specificity of growing Au on hybrid ZnS-CdS nanostructures with the gold only on CdS domains.

the composition profile of the as-prepared ZnS-CdS, EDS line analysis was applied. As shown in Figure 1e (also in Figure S9), the element composition distributions were investigated along the [111] zone axes (inset of Figure 1e). The result demonstrates that Zn and S enrich the entire rod, while Cd distributes in a section-by-section manner (i.e., node sheaths of hetero-nanorods). The multi-node sheath characteristics were further evidenced by the element maps (Figure 1f). Peaks appearing in the XRD spectrum (Figure S10a) can be attributed to a combination of cubic ZnS (JCPDS No. 65-0309) and cubic CdS (JCPDS No. 65-2887). The molar ratio of Cd and Zn elements after exchange, identified by EDS measurement (Figure S10b), indicates that almost all the $Ag^{+}$ ions were exchanged by $Cd^{2+}$. XPS peaks corresponded well with ZnS and CdS, also reflecting the occurrence of cation exchange between Ag and Cd (Figure S10c–f).

Sophisticated architectures of building complexity are required for nanostructures to fulfill their expanding applications, which incites researchers to explore the construction of more components in one single structure.[3a] Furthermore, rational arrangement of component domains may promote the cooperative processes within the nanocrystals that facilitate enhanced functionality. Ternary ZnS-(CdS/metal) heterostructures were prepared through the post-synthetic modification of pre-made multi-node sheath binary ZnS-CdS hetero-nanorods. In a typical synthesis of Au nanocrystals, a quantity of multi-node sheath ZnS-CdS was added at the initial stage of reaction as seeds to obtain the surface growth. As shown in Figure 2b (large-field view in Figure S11), Au nanoparticles prefer to nucleate on CdS node sheaths but not on ZnS stems (Figure 2b–g). High-resolution STEM images in Figure 2f and Figure S12 reveal the planes of these three components. XRD pattern (Figure S13a) and EDS spectrum (Figure S13b) show the Au peaks. EDS mapping images (Figure 2g) clarify the composition profile and further demonstrate the regiospecificity for growing Au on hybrid ZnS-CdS nanostructures with metal being grown only on CdS domains. The effect of the precursor ratio on the morphology of ZnS-(CdS/Au) hybrids is shown (Figure S14). With increasing amounts of Au precursor, Au nanoparticles grow on the CdS domains as before, and become bigger through the Ostwald ripening process. Similar results were obtained for the selectively heterogeneous nucleation of Pd or Pt on the binary hetero-nanorods by reducing $Pd(acac)_2$ or $Pt(acac)_2$ in the presence of the ZnS-CdS seeds, which formed exclusive ZnS-(CdS/Pd) (Figure S15) or ZnS-(CdS/Pt) (Figure S16). Herein we chose Au, Pd, and Pt loadings for achieving selective deposition on CdS($\bar{1}10$) surface instead of on ZnS($\bar{1}10$). The ($\bar{1}10$) surfaces of Au, Pd, and Pt have similar lattice constants (Table S1). Whereas three unit cells of Au, Pd, or, Pt can form compatible lattice matching with two CdS($\bar{1}10$) units, the ZnS($\bar{1}10$) facet requires three unit cells to achieve matching with four Au, Pd, or Pt cells. This difference explains why metals form good interfaces with CdS($\bar{1}10$) instead of with ZnS($\bar{1}10$) in the synthesis.

To demonstrate the rationality of designed hetero-nanostructures, we examined the material bandgap alignment in theory. In terms of the binary system, as the ZnS nanorod grows along the [111] direction, its side facet should be ($\bar{1}10$) in contact with CdS($\bar{1}10$) (Figure S17a). The computed work-functions of ZnS($\bar{1}10$) and CdS($\bar{1}10$) are quite close (Figure S17b), implying a well contacted and coupled interface. The computed DOS distributions (Figure S17c) suggest a straddling band alignment (type I) between ZnS($\bar{1}10$) and CdS($\bar{1}10$). In fact, our binary multi-node sheath nanostructure can be treated as a ZnS(111) nanorod attached by ZnS($\bar{1}10$)/CdS($\bar{1}10$) hybrid node sheaths. By optimizing the ZnS($\bar{1}10$)/


© 2015 Wiley-VCH Verlag GmbH & Co. KGaA, Weinheim

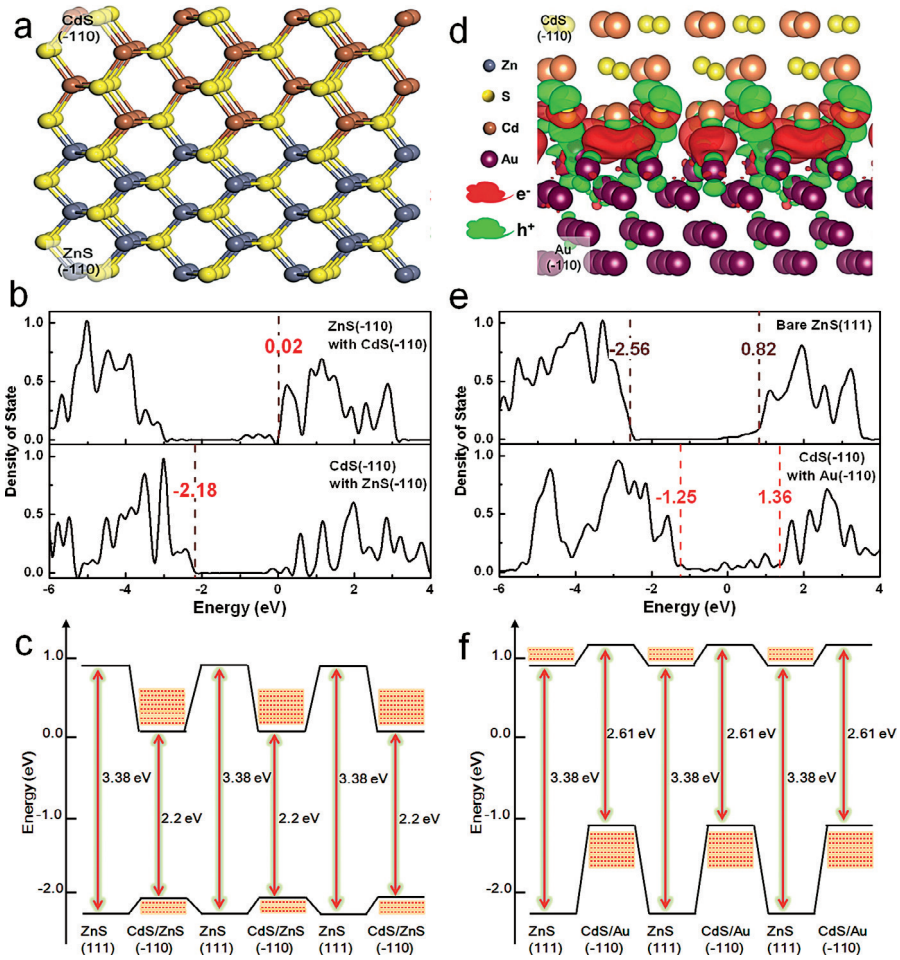


***Figure 3.*** a) The atomic model at the interface of ZnS($\bar{1}10$)/CdS($\bar{1}10$) hybrid. b) The computed partial density of states (DOS) for the ZnS and CdS parts at the ZnS($\bar{1}10$)-CdS($\bar{1}10$) interface. c) The energy-band alignment of a ZnS(111) nanorod attached by the ZnS($\bar{1}10$)/CdS($\bar{1}10$) hybrid in the periodic binary heterojunction. d) The simulated charge distributions at the CdS($\bar{1}10$)/Au interface. e) The simulated DOS of bare ZnS(111) and CdS($\bar{1}10$)/Au($\bar{1}10$) hybrid, suggesting a staggered bandgap alignment. f) The energy-band alignment of the periodic ternary heterojunction with CdS($\bar{1}10$)/Au hybrids attached to a ZnS(111) nanorod.

CdS($\bar{1}10$) potential lineup (Figure S17d) and interface model (Figure 3a), we learned from calculated DOS (Figure 3b) that the energy gap of ZnS($\bar{1}10$)/CdS($\bar{1}10$) locates inside that of ZnS(111). The ZnS-CdS hetero-nanorod thus constitutes a periodic straddling gap alignment (Figure 3c), which unfortunately suffers from undesired electron and hole accumulation at the purely CdS parts.

In terms of the ternary system, the computed workfunction of CdS($\bar{1}10$) is about 1.0 eV larger than those of the ($\bar{1}10$) surfaces of Au (5.02 eV), Pd (4.92 eV), and Pt (5.20 eV). Thus the Fermi level/workfunction difference established drives free electrons to flow from Au, Pd, or Pt into CdS($\bar{1}10$), bending the CdS bands. Simulations indicated that one Au($\bar{1}10$) unit cell donates 0.84 electrons to CdS($\bar{1}10$) (Figure 3d), decreasing the workfunction from 5.95 to 5.03 eV (Figure S18). This implies that the Fermi level and energy bands of CdS($\bar{1}10$) might also be levitated by about 0.90 eV, becoming ready for staggered gap alignment with ZnS($\bar{1}10$) and ZnS(111). Simulations also revealed the electronic structure (DOS) of CdS($\bar{1}10$)/Au hybrid (Figure 3e), in which the valence and conduction band edges of the bare CdS($\bar{1}10$) are leveled up by Au-donated electrons from −2.18 to −1.25 eV and from 0.02 to 1.36 eV, respectively. As expected, this results in periodic staggered gaps when aligning with the bands of the ZnS-(111) nanorod (Figure 3f). Therefore, photo-generated electrons will be delivered to both Au and ZnS-(111), and holes will accumulate at CdS($\bar{1}10$). Meanwhile, the gaps of ZnS(111) and CdS($\bar{1}10$) still cover the reaction potentials for water splitting and correspond to ultraviolet and visible light absorption, making our design an ideal system for photocatalytic water splitting.

The optical spectra of the synthesized ZnS nanorods, binary multinode sheath ZnS-CdS hetero-nanorods, and ternary ZnS-(CdS/Au) are characterized by UV/Vis-near infrared (NIR) absorption and photoluminescence (PL) emission spectra. The initial ZnS nanorods show discernible UV absorption positions corresponding to the ZnS bandgap (ca. 3.6 eV). In the absorption spectrum of ZnS-CdS, the shoulder at around 485 nm is attributed to the excitonic absorption of CdS (ca. 2.4 eV). Compared with binary ZnS-CdS, ternary ZnS-(CdS/Au) has a certain degree of red shift (Figure 4a). It is reasonable to expect that the ternary ZnS-(CdS/Au) system, with respect to the two binary systems ZnS-CdS and CdS/Au as well as to the bare ZnS and bare CdS, could perform well in terms of suppression of electron–hole recombination. Indeed, this expectation was verified as shown by a careful comparison of the photoluminescence (PL) emission spectra (excitation at 400 nm) recorded on samples that contain the same amount (in weight) of CdS nanocrystals. As clearly seen from Figure 4b, the broad PL emissions in the visible region, known to originate from the trap (or defect) states of CdS, were drastically quenched for ZnS-(CdS/Au), in contrast to ZnS-CdS, CdS/Au, or bare CdS. This set of crude (yet rational) PL measurements discloses, to a certain extent, the high caliber of our ZnS-(CdS/Au) system in suppressing the electron–hole recombination.

On the basis of the information obtained, it is not surprising for us to achieve better optical-to-electrical conversion by implementing the well-designed ternary structure. As a proof-of-concept demonstration, our examination on photocatalytic water splitting (Figure 4c,d) indicated that the hydrogen-production rates (per catalyst weight) are in the


© 2015 Wiley-VCH Verlag GmbH & Co. KGaA, Weinheim

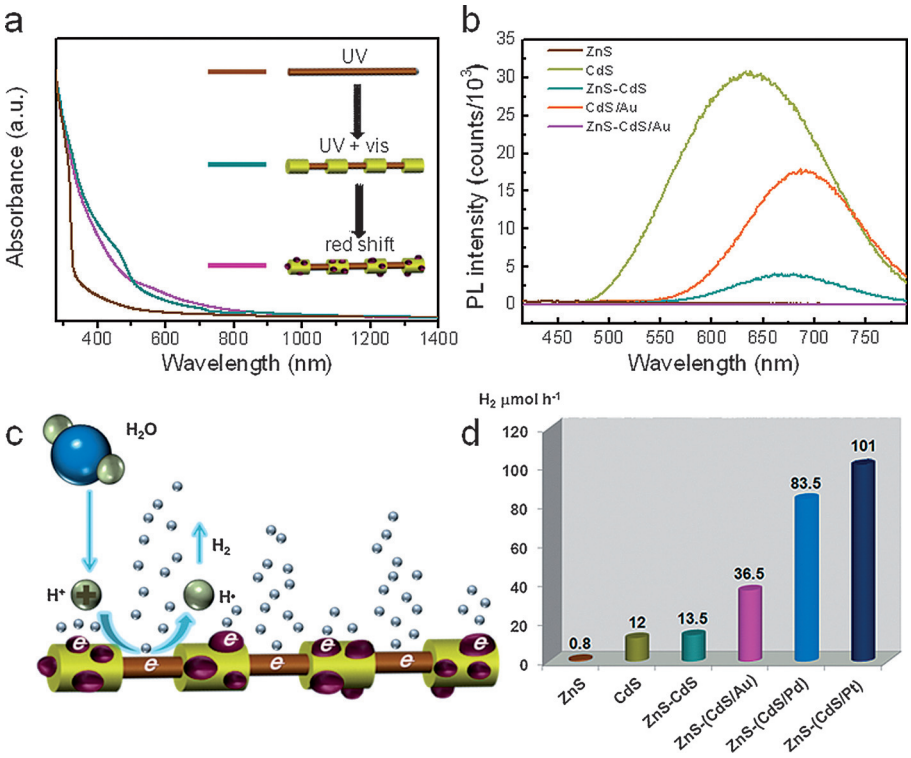


***Figure 4.*** a) Absorption spectra for colloidal nanocrystals of single ZnS nanorods (brown), binary ZnS-CdS hetero-nanorods (green) and ternary ZnS-(CdS/Au) hetero-nanorods (red). b) Photoluminescence (PL) spectroscopic characterization for the five nanosystems as annotated within the plot. c) Schematic representation of the photocatalytic generation of $H_2$. d) Comparison of $H_2$ evolution rates under visible-light irradiation using different photocatalysts.

order of ZnS-(CdS/Au) > ZnS-CdS≅bare CdS > bare ZnS. We also investigated the cycles of photocatalytic hydrogen evolution (Table S2). The substitution of Au with Pd or Pt in the ternary structure brought about further improvement in photocatalysis efficiency. To illustrate this result, we have also examined the band-engineering efficacy by substituting Au with Pd or Pt in the ternary system. Simulations predicted that Pd and Pt have deeper potential wells than Au (Figure S19), thus the unit cells of Pd and Pt donate more electrons to the CdS($\bar{1}$10) part (Figure S19b). It is worth mentioning that the photocatalytic hydrogen evolution with different amounts of Au deposition was also evaluated (Figure S20).

We have also successfully synthesized a series of multi-node sheath chalcogenide hetero-nanorods (e.g., ZnS-ZnS and ZnS-PbS) by sequential cation exchange at room temperature (Figure S21,22), as we envision that the ternary system of S1-(S2/M) featuring selective growth of metal on one semiconductor may be extended when starting from other multi-node sheath heterostructures; further work along this line is under way in our laboratory.

In summary, we have successfully developed a facile and general colloidal method for the construction of ultrathin 1D binary and ternary multi-node sheath hetero-nanorods. This strategy, based on the cation exchange and post-synthetic modification, offers advantages over conventional hot-injection methods for the synthesis of hetero-nanostructures. The transformation from binary ZnS-CdS hetero-nanorod to ternary ZnS-(CdS/metal) hetero-nanorod with segmented node sheaths decorated by metal nanoparticles is a useful tactic for preparing type-II heterojunctions from type-I. The separation of electron–hole pairs is a critical step to nearly all applications involving semiconductor materials; hence the strategy reported herein provides fresh insights into energy-band engineering in which appropriate components enhancing their functionalities synergistically. The optimization of system nanosizes, as well as the adjustment of the metal and semiconductor content, may offer opportunities to improve their optoelectronic performances. Moreover, the use of theoretical characterizations to guide the optimization of photocatalysis has also been demonstrated in this study. We anticipate that this work opens a new door to rationally designing hybrid systems for photo-induced applications.

## Acknowledgements

This work is supported by the National Natural Science Foundation of China (Grants 21431006, 91227103, 21061160492, J1030412, 91221104, 91127042, 21173205), the Ministry of Science and Technology of China (Grants 2013CB933900, 2014CB931800, 2014CB848900, 2010CB923300), the Chinese Academy of Sciences (Grant KJZD-EW-M01-1), the CAS Strategic Priority Research Program B (No. XDB01020000), and the China Recruitment Program of Global Expert.

**Keywords:** charge separation · chemical transformation · hetero-nanorods · photocatalysis · ternary ZnS-(CdS/metal)

**How to cite:** *Angew. Chem. Int. Ed.* **2015**, *54*, 11495–11500
*Angew. Chem.* **2015**, *127*, 11657–11662

[1] a) X. Peng, L. Manna, W. Yang, J. Wickham, E. Scher, A. Kadavanich, A. P. Alivisatos, *Nature* **2000**, *404*, 59–61; b) Y. Xia, Y. Xiong, B. Lim, S. E. Skrabalak, *Angew. Chem. Int. Ed.* **2009**, *48*, 60–103; *Angew. Chem.* **2009**, *121*, 62–108; c) Y. Du, Z. Yin, J. Zhu, X. Huang, X. J. Wu, Z. Zeng, Q. Yan, H. Zhang, *Nat. Commun.* **2012**, *3*, 1177; d) D. K. Harris, M. G. Bawendi, *J. Am. Chem. Soc.* **2012**, *134*, 20211–20213; e) M. H. Oh, T. Yu, S.-H. Yu, B. Lim, K.-T. Ko, M.-G. Willinger, D.-H. Seo, B. H. Kim, M. G. Cho, J.-H. Park, K. Kang, Y.-E. Sung, N. Pinna, T. Hyeon, *Science* **2013**, *340*, 964–968; f) D. Wang, H. L. Xin, R. Hovden, H. Wang, Y. Yu, D. A. Muller, F. J. DiSalvo, H. D. Abruña, *Nat. Mater.* **2013**, *12*, 81–87; g) X. Pang, C. Wan, M. Wang, Z. Lin, *Angew. Chem. Int. Ed.* **2014**, *53*, 5524–5538; *Angew. Chem.* **2014**, *126*, 5630–5644; h) L. Wang, J. Ge, A. Wang, M. Deng, X. Wang, S. Bai, R. Li, J. Jiang, Q. Zhang, Y. Luo, Y. Xiong, *Angew. Chem. Int. Ed.*

 © 2015 Wiley-VCH Verlag GmbH & Co. KGaA, Weinheim 

**2014**, *53*, 5107 – 5111; *Angew. Chem.* **2014**, *126*, 5207 – 5211; i) E. Lhuillier, S. Pedetti, S. Ithurria, B. Nadal, H. Heuclin, B. Dubertret, *Acc. Chem. Res.* **2015**, *48*, 22 – 30; j) C. Tan, H. Zhang, *Chem. Soc. Rev.* **2015**, *44*, 2713 – 2731.

[2] a) R. Costi, A. E. Saunders, U. Banin, *Angew. Chem. Int. Ed.* **2010**, *49*, 4878 – 4897; *Angew. Chem.* **2010**, *122*, 4996 – 5016; b) G. D. Moon, S. Ko, Y. Min, J. Zeng, Y. Xia, U. Jeong, *Nano Today* **2011**, *6*, 186 – 203; c) X. W. Liu, D. S. Wang, Y. D. Li, *Nano Today* **2012**, *7*, 448 – 466; d) Y. Yin, D. Talapin, *Chem. Soc. Rev.* **2013**, *42*, 2484 – 2487; e) T. Simon, N. Bouchonville, M. J. Berr, A. Vaneski, A. Adrovic, D. Volbers, R. Wyrwich, M. Doblinger, A. S. Susha, A. L. Rogach, F. Jackel, J. K. Stolarczyk, J. Feldmann, *Nat. Mater.* **2014**, *13*, 1013 – 1018; f) B. Xu, P. He, H. Liu, P. Wang, G. Zhou, X. Wang, *Angew. Chem. Int. Ed.* **2014**, *53*, 2339 – 2343; *Angew. Chem.* **2014**, *126*, 2371 – 2375; g) Z.-c. Zhang, B. Xu, X. Wang, *Chem. Soc. Rev.* **2014**, *53*, 2339 – 2343; h) M. R. Gao, J. X. Liang, Y. R. Zheng, Y. F. Xu, J. Jiang, Q. Gao, J. Li, S. H. Yu, *Nat. Commun.* **2015**, *6*, 5982 – 5988.

[3] a) M. T. Mayer, Y. Lin, G. Yuan, D. Wang, *Acc. Chem. Res.* **2013**, *46*, 1558 – 1566; b) Y. Qu, X. Duan, *Chem. Soc. Rev.* **2013**, *42*, 2568 – 2580.

[4] L. Carbone, P. D. Cozzoli, *Nano Today* **2010**, *5*, 449 – 493.

[5] a) X. Wang, J. Zhuang, Q. Peng, Y. Li, *Nature* **2005**, *437*, 121 – 124; b) Y. Yin, A. P. Alivisatos, *Nature* **2005**, *437*, 664 – 670; c) Z. Zhuang, Q. Peng, Y. Li, *Chem. Soc. Rev.* **2011**, *40*, 5492 – 5513.

[6] a) D. H. Son, S. M. Hughes, Y. Yin, A. P. Alivisatos, *Science* **2004**, *306*, 1009 – 1012; b) J. B. Rivest, P. K. Jain, *Chem. Soc. Rev.* **2013**, *42*, 89 – 96.

[7] P. K. Jain, L. Amirav, S. Aloni, A. P. Alivisatos, *J. Am. Chem. Soc.* **2010**, *132*, 9997 – 9999.

[8] a) R. D. Robinson, B. Sadtler, D. O. Demchenko, C. K. Erdonmez, L.-W. Wang, A. P. Alivisatos, *Science* **2007**, *317*, 355 – 358; b) B. Sadtler, D. O. Demchenko, H. Zheng, S. M. Hughes, M. G. Merkle, U. Dahmen, L.-W. Wang, A. P. Alivisatos, *J. Am. Chem. Soc.* **2009**, *131*, 5285 – 5293; c) Y. Justo, B. Goris, J. S. Kamal, P. Geiregat, S. Bals, Z. Hens, *J. Am. Chem. Soc.* **2012**, *134*, 5484 – 5487.

[9] A. E. Martell, R. D. Hancock, Metal Complexes in Aqueous Solutions, Plenum Press, New York, **1996**.

Received: June 13, 2015
Published online: August 14, 2015


© 2015 Wiley-VCH Verlag GmbH & Co. KGaA, Weinheim